The Astrophysical Journal, 679:1029–1039, 2008 June 1

SIMULTANEOUS MULTIWAVELENGTH OBSERVATIONS OF THE BLAZAR 1ES 1959+650 AT A LOW TeV FLUX

G. Tagliaferri,[1] L. Foschini,[2] G. Ghisellini,[1] L. Maraschi,[3] and G. Tosti[4]

and

J. Albert,[5] E. Aliu,[6] H. Anderhub,[7] P. Antoranz,[8] C. Baixeras,[9] J. A. Barrio,[8] H. Bartko,[10] D. Bastieri,[11] J. K. Becker,[12] W. Bednarek,[13] A. Bedyugin,[14] K. Berger,[5] C. Bigongiari,[11] A. Biland,[7] R. K. Bock,[10,11] P. Bordas,[15] V. Bosch-Ramon,[15] T. Bretz,[5] I. Britvitch,[7] M. Camara,[8] E. Carmona,[10] A. Chilingarian,[16] J. A. Coarasa,[10] S. Commichau,[7] J. L. Contreras,[8] J. Cortina,[6] M. T. Costado,[17,18] V. Curtef,[12] V. Danielyan,[16] F. Dazzi,[11] A. De Angelis,[19] C. Delgado,[17] R. de los Reyes,[8] B. De Lotto,[19] D. Dorner,[5] M. Doro,[11] M. Errando,[6] M. Fagiolini,[20] D. Ferenc,[21] E. Fernández,[6] R. Firpo,[6] M. V. Fonseca,[8] L. Font,[9] M. Fuchs,[10] N. Galante,[10] R. J. García-López,[17,18] M. Garczarczyk,[10] M. Gaug,[17] M. Giller,[13] F. Goebel,[10] D. Hakobyan,[16] M. Hayashida,[10] T. Hengstebeck,[22] A. Herrero,[17,18] D. Höhne,[5] J. Hose,[10] S. Huber,[5] C. C. Hsu,[10] P. Jacon,[13] T. Jogler,[10] R. Kosyra,[10] D. Kranich,[7] R. Kritzer,[5] A. Laille,[21] E. Lindfors,[14] S. Lombardi,[11] F. Longo,[19] M. López,[8] E. Lorenz,[7,10] P. Majumdar,[10] G. Maneva,[23] K. Mannheim,[5] M. Mariotti,[11] M. Martínez,[6] D. Mazin,[6] C. Merck,[10] M. Meucci,[20] M. Meyer,[5] J. M. Miranda,[8] R. Mirzoyan,[10] S. Mizobuchi,[10] A. Moralejo,[6] D. Nieto,[8] K. Nilsson,[14] J. Ninkovic,[10] E. Oña-Wilhelmi,[6] N. Otte,[10,22] I. Oya,[8] M. Panniello,[17,24] R. Paoletti,[20] J. M. Paredes,[15] M. Pasanen,[14] D. Pascoli,[11] F. Pauss,[7] R. Pegna,[20] M. Persic,[19,25] L. Peruzzo,[11] A. Piccioli,[20] E. Prandini,[11] N. Puchades,[6] A. Raymers,[16] W. Rhode,[12] M. Ribó,[15] J. Rico,[6] M. Rissi,[7] A. Robert,[9] S. Rügamer,[5] A. Saggion,[11] T. Y. Saito,[10] A. Sánchez,[9] P. Sartori,[11] V. Scalzotto,[11] V. Scapin,[19] R. Schmitt,[5] T. Schweizer,[10] M. Shayduk,[10,22] K. Shinozaki,[10] S. N. Shore,[26] N. Sidro,[6] A. Sillanpää,[14] D. Sobczynska,[13] F. Spanier,[5] A. Stamerra,[20] L. S. Stark,[7] L. Takalo,[14] F. Tavecchio,[1] P. Temnikov,[23] D. Tescaro,[6] M. Teshima,[10] D. F. Torres,[27] N. Turini,[20] H. Vankov,[23] A. Venturini,[11] V. Vitale,[19] R. M. Wagner,[10] T. Wibig,[13] W. Wittek,[10] F. Zandanel,[11] R. Zanin,[6] and J. Zapatero[9]

(The MAGIC Collaboration)

Received 2007 December 3; accepted 2008 January 24

ABSTRACT

We present the results from a multiwavelength campaign on the TeV blazar 1ES 1959+650, performed in 2006 May. Data from the optical, UV, soft- and hard-X-ray, and very high energy (VHE) gamma-ray ($E > 100$ GeV) bands were obtained with the *Suzaku* and *Swift* satellites, the MAGIC telescope, and other ground-based facilities. The source spectral energy distribution (SED), derived from *Suzaku* and MAGIC observations at the end of 2006 May, shows the usual double hump shape, with the synchrotron peak at a higher flux level than the Compton peak. With respect to historical values, during our campaign the source exhibited a relatively high state in X-rays and optical, while in the VHE band it was at one of the lowest level so far recorded. We also monitored the source for flux spectral variability on a time window of 10 days in the optical-UV and X-ray bands and 7 days in the VHE band. The source varies more in the X-ray than in the optical band, with the 2–10 keV X-ray flux varying by a factor of ∼2. The synchrotron peak is located in the X-ray band and moves to higher energies as the source gets brighter, with the X-ray fluxes above it varying more rapidly than the X-ray fluxes at lower energies. The variability behavior observed in the X-ray band cannot be

[1] INAF/Osservatorio Astronomico di Brera, via Bianchi 46, 23807 Merate (LC), Italy.
[2] INAF/IASF-Bologna, Via Gobetti 101, 40129 Bologna, Italy.
[3] INAF/Osservatorio Astronomico di Brera, via Brera 28, 20121 Milano, Italy.
[4] Osservatorio Astronomico, Università di Perugia, Via B. Bonfigli, 06126 Perugia, Italy.
[5] Universität Würzburg, D-97074 Würzburg, Germany.
[6] IFAE, Edifici C, E-08193 Bellaterra (Barcelona), Spain.
[7] ETH Zurich, CH-8093 Switzerland.
[8] Universidad Complutense, E-28040 Madrid, Spain.
[9] Universitat Autònoma de Barcelona, E-08193 Bellaterra, Spain.
[10] Max-Planck-Institut für Physik, D-80805 München, Germany.
[11] Università di Padova and INFN, I-35131 Padova, Italy.
[12] Universität Dortmund, D-44227 Dortmund, Germany.
[13] University of Łódź, PL-90236 Lodz, Poland.
[14] Tuorla Observatory, Turku University, FI-21500 Piikkiö, Finland.
[15] Universitat de Barcelona, E-08028 Barcelona, Spain.
[16] Yerevan Physics Institute, AM-375036 Yerevan, Armenia.
[17] Institute de Astrofisica de Canarias, E-38200, La Laguna, Tenerife, Spain.
[18] Departamento de Astrofisica, Universidad de La Leguna, E-38206 La Laguna, Tenerife, Spain.
[19] Università di Udine, and INFN Trieste, I-33100 Udine, Italy.
[20] Università di Siena, and INFN Pisa, I-53100 Siena, Italy.
[21] University of California, Davis, CA 95616-8677.
[22] Humboldt-Universität zu Berlin, D-12489 Berlin, Germany.
[23] Institute for Nuclear Research and Nuclear Energy, BG-1784 Sofia, Bulgaria.
[24] Deceased.
[25] INAF/Osservatorio Astronomico and INFN, I-34131 Trieste, Italy.
[26] Università di Pisa, and INFN Pisa, I-56126 Pisa, Italy.
[27] ICREA and Institut de Cienciès de l'Espai (IEEC-CSIC), E-08193 Bellaterra, Spain.

produced by emitting regions varying independently and suggests instead some sort of "standing shock" scenario. The overall SED is well represented by a homogeneous one-zone synchrotron inverse Compton emission model, from which we derive physical parameters that are typical of high-energy peaked blazars.

Subject headings: BL Lacertae objects: individual (1ES 1959+650) — galaxies: active — galaxies: jets — X-rays: galaxies

Online material: color figures

1. INTRODUCTION

It is widely accepted that the spectral energy distribution (SED) of blazars is dominated by a nonthermal continuum, produced within a relativistic jet closely aligned with the line of sight, making these objects very good laboratories to study the physics of relativistic jets. The overall emission, from radio to γ-rays and, in some cases, to the multi-TeV band, shows the presence of two well-defined broad components (von Montigny et al. 1995; Fossati et al. 1998). Usually, for the blazars that are detected in the TeV bands, the first components peaks in the UV–soft-X-ray bands (high-energy peaked blazars [HBLs]; Padovani & Giommi 1995) and the second one in the GeV-TeV region. The blazar emission is very successfully interpreted so far in the framework of synchrotron inverse Compton (IC) models. The lower energy peak is unanimously attributed to synchrotron emission by relativistic electrons in the jet, while the second component is commonly believed to be IC emission from the same electron population (e.g., Ghisellini et al. 1998), although different scenarios have been proposed (e.g., Böttcher 2007).

Since the discovery of the first blazar emitting TeV radiation, Mrk 421 (Punch et al. 1992), TeV blazars have been the target of intense observational and theoretical investigations. Indeed, the possibility of coupling observations of the emission produced by very high energy (VHE) electrons, in the VHE band (up to Lorentz factors of the order of 10^7), with observations in the soft and hard X-ray bands, offers a unique tool to probe the cooling and acceleration processes of relativistic particles. In fact, the synchrotron peak of these sources is usually located in the soft X-ray, while it is in the hard X-ray band that the synchrotron emission by the most energetic electrons can be studied and that the low-energy part of the Compton emission component can start to dominate.

Studies conducted simultaneously in the soft and hard X-ray and in the VHE bands are of particular importance, since in the simple synchrotron self-Compton (SSC) framework one expects that variations in X-rays and TeV should be closely correlated, being produced by the same electrons (e.g., Tavecchio et al. 1998). In fact, even the first observations at X-ray and TeV energies yielded significant evidence of correlated and simultaneous variability of the TeV and X-ray fluxes (Buckley et al. 1996; Catanese et al. 1997). During the X-ray/TeV 1998 campaign on Mrk 421, a rapid flare was detected at both X-ray and TeV energies (Maraschi et al. 1999). Subsequent observations confirmed these first evidences also in other sources. Note, however, that the correlation seems to be violated in some cases, as indicated by the observation of an "orphan" (i.e., not accompanied by a corresponding X-ray flare) TeV event in 1ES 1959+650 (Krawczynski et al. 2004). In the case of PKS 2155−304 a giant TeV flare recorded by H.E.S.S. (Aharonian et al. 2007), with a TeV flux "night-average" intensity of a factor of $\sim$17 larger than those of previous campaigns, was accompanied by an increase of the X-ray flux of only a factor of 5 without a significant change of the X-ray spectrum (Foschini et al. 2007). In the one-zone SSC scenario this can be accomplished with an increase of the Doppler factor and the associated relativistic electrons together with a decrease of the magnetic field. Therefore, it is important to obtain simultaneous observations over the largest possible UV and X-ray range together with simultaneous VHE observation to probe the correlation between the synchrotron and VHE emission.

To this end we organized a multiwavelength campaign to observe the blazar 1ES 1959+650 in the optical, UV, and soft and hard X-ray up to the VHE gamma-ray ($E > 100$ GeV) bands. This is a bright and flaring X-ray and VHE source that has already been observed many times in these bands. It was discovered in the radio band as part of a 4.85 GHz survey performed with the 91 m NRAO Green Bank telescope (Gregory & Condon 1991; Becker et al. 1991). In the optical band it is highly variable and shows a complex structure composed by an elliptical galaxy ($M_R = -23$, $z = 0.048$) plus a disk and an absorption dust lane (Heidt et al. 1999). The mass of the central black hole has been estimated to be in the range $(1.3–4.4) \times 10^8\ M_\odot$ as derived from either the stellar velocity dispersion or the bulge luminosity (Falomo et al. 2002). The first X-ray measurement was performed by *Einstein* IPC during the Slew Survey (Elvis et al. 1992). Subsequently, the source was observed by *ROSAT*, *BeppoSAX*, *RXTE*, *ARGOS*, and *XMM-Newton*. In particular, two *BeppoSAX* pointings, simultaneous with optical observations, were triggered in 2002 May–June because the source was in a high X-ray state. These data showed that the synchrotron peak was in the range 0.1–0.7 keV and that the overall optical and X-ray spectrum up to 45 keV was due to synchrotron emission with the peak moving to higher energy with the higher flux (Tagliaferri et al. 2003). The overall SED, with nonsimultaneous VHE data, could be modeled with a homogeneous, one-zone synchrotron inverse Compton model. The results of a multiwavelength campaign performed in 2003 May–June are presented in Gutierrez et al. (2006). This campaign was triggered by the active state of the source in the X-ray band, and it was found that the X-ray flux and X-ray photon index are correlated. A similar result was found by Giebels et al. (2002) using *RXTE* and *ARGOS* data. This correlation shows that the X-ray spectrum in the 1–16 keV band is harder when the source is brighter. In the VHE band the source was detected by the HEGRA, Whipple, and MAGIC telescopes (Aharonian et al. 2003; Holder et al. 2003a; Albert et al. 2006). One of the most important results of these observations is probably the "orphan" flare mentioned above, seen in the VHE band and not in X-rays (Krawczynski et al. 2004).

1ES 1959+650 is therefore one of the most interesting and frequently observed high-energy sources of recent years. With the aim of obtaining a better description of the broadband X-ray continuum and in particular of observing simultaneously the synchrotron and IC components, we asked for simultaneous *Suzaku* and MAGIC observations that were carried out in 2006 May 23–25. Around the same epoch we obtained various Target of Opportunity (ToO) short pointings with *Swift* and observed the source also in the optical *R* band from ground. A preliminary analysis of these data is reported in Hayashida et al. (2008). In the following we report the data analysis (§ 2) and the results (§ 3). The discussion and conclusions are given in § 4, where we model

TABLE 1
BEST-FIT PARAMETERS FOR THE XIS DATA OF THE WHOLE *Suzaku* OBSERVATION

Model (1)	Γ or Γ_1 or a (2)	$N_{\rm H}$ or Γ_2 or b (3)	E_b or E_{b1} (4)	Γ_3 (5)	E_{b2} (6)	χ^2_r/dof (7)	F_{2-10} (8)
			Suzaku XIS				
pl+A	2.197 ± 0.001	$1.555^{+0.002}_{-0.001}$	...	...	...	0.96/5455	2
bpl+GA	1.958 ± 0.003	$2.205^{+0.03}_{-0.01}$	1.83 ± 0.01	...	...	1.01/5454	2
log-par	1.96 ± 0.01	0.20 ± 0.01	...	...	...	0.99/5456	2
			Suzaku XIS+HXD/PIN				
2-bpl+GA	1.94 ± 0.001	2.195 ± 0.02	1.83 ± 0.03	2.7 ± 0.03	16 ± 3	0.97/4183	2
log-par	1.95 ± 0.01	0.21 ± 0.01	...	...	...	0.98/4186	2

NOTES.—Col. (1): Model used to fit the XIS data (pl=power law; bpl=broken power law; log-par=log-parabolic law; GA=absorption fixed at the Galactic value, $N_{\rm H} = 10^{21}$ cm^{-2}; A: free absorption in the source rest frame). Col. (2): Photon index for the pl model, or low-energy photon index for the bpl model, or log-parabolic slope. Col. (3): Value of the $N_{\rm H}$ (in units of 10^{21} cm^{-2}), or high-energy photon index for the bpl model, or log-parabolic curvature. Col. (4): Break energy (keV) for the bpl model. Col. (5): Third photon index for the 2-bpl model. Col. (6): Second break energy (keV) for the 2-bpl model. Col. (7): χ^2/degrees of freedom. Col. (8): Flux in the 2–10 keV band, in units of 10^{-10} erg cm^{-2} s^{-1}.

the SED in the framework of a homogeneous, one-zone SSC model. Throughout this work we use $H_0 = 70$ km s^{-1} Mpc^{-1}, $\Omega_\Lambda = 0.7$, $\Omega_M = 0.3$.

2. OBSERVATIONS AND DATA REDUCTION

2.1. *Suzaku*

The *Suzaku* payload (Mitsuda et al. 2007) carries four X-ray telescopes sensitive in the 0.3–12 keV band (XIS; Koyama et al. 2007), with CCD cameras in the focal plane, together with a nonimaging instrument (HXD; Takahashi et al. 2007), sensitive in the 10–600 keV band, composed of a Si-PIN photodiode detector (probing the 10–60 keV band) and a GSO scintillator detector (sensitive above 30 keV). Three XIS units (XIS0, 2, and 3) have front-illuminated CCDs, while XIS1 uses a back-illuminated CCD, more sensitive at low energies.

1ES 1959+650 was observed from 2006 May 23 01:13:23 UT to May 25 04:07:24 UT (sequence number 701075010). The total on-source time was 160 ks.

The HXD/PIN light curve shows a rapid increase of the noise after ~100 ks (possibly due to the in-orbit radiation damage),[28] and the data after this event cannot be used for the analysis. HXD/GSO data are not used in the following analysis, since the performances and the background of the GSO are still under study.

The analysis was performed with the data obtained through the last version of the processing (ver. 1.2) and the last release of the HEASoft software (ver. 6.1.2) and calibrations. A more extended discussion of the procedure used can be found in Tavecchio et al. (2007).

2.1.1. *Suzaku-XIS*

The reduction of the XIS data followed the prescriptions reported in The Suzaku Data Reduction Guide.[29] Using the HEASoft tool `xselect` we select good time intervals, excluding epochs of high background (when the satellite crosses the South Atlantic Anomaly or the object is too close to the rim of the Earth). After screening the net exposure time is 99.3 ks. During the observation the source shows a flare of small amplitude with rather small spectral variability (see below); therefore, we extracted the spectra corresponding to the whole observation. Events are then extracted in a circle centered on the source with a radius of 6′. Background events are extracted in a similar circle centered in a region devoid of sources. We checked that the use of different source and background regions do not significantly affect the resulting spectra. Response (redistribution matrix file [RMF]) and auxiliary (ancillary response file [ARF]) files are produced using the tools developed by the *Suzaku* team (`xisrmfgen` and `xissimarfgen`) distributed with the last version of HEASoft. ARFs are already corrected for the degradation of the XIS response using the tool `xiscontamicalc`.

For the spectral analysis we use the XIS data in the range 0.7–10 keV. Below 0.7 keV there are still unsolved calibration problems. Due to the high signal-to-noise ratio of the data the residuals of the fits also reveal the presence of a deep edge around 1.8 keV, whose origin is clearly instrumental. Therefore, we perform the fits excluding the data points in the range 1.7–2 keV. A power-law (PL) continuum with Galactic absorption gives unacceptable results. If we allow the absorption to vary, we obtain a good fit to the data ($\chi^2_r = 1.01$), but the value of the $N_{\rm H}$ is significantly in excess of the Galactic value of 1×10^{21} cm^{-2}. However, given that we do not expect to have intrinsic absorption in this source, while we do expect to see a bending of the X-ray spectrum over this energy range (e.g., Tagliaferri et al. 2003; Tramacere et al. 2007), we also fitted a broken-PL model with the absorption fixed to the Galactic value. This model provides a good fit to the data with a break at ~1.8 keV (note that this is also confirmed by the analysis of the *Swift*-XRT data [see § 2.2.1]; therefore, this is not due to the instrument feature mentioned above). Clearly, the X-ray spectrum of 1ES1959+650 is showing a curvature; therefore, we also fitted a log-parabolic law model that provides a good description of HBL X-ray spectra (Massaro et al. 2004; Donato et al. 2005). Indeed, this model also provides a good fit with the absorption fixed to the Galactic value (see Table 1 for a summary of the best-fit results).

2.1.2. *Suzaku HXD/PIN*

The HXD/PIN data are reduced following the procedure suggested by the *Suzaku* team. The HXD/PIN spectrum is extracted after the selection of good time intervals (analogously to the XIS procedure). To the extracted spectrum (obtained through `xselect`) we applied the suggested dead-time correction (of the order of 5%). The net exposure time after screening is 40.2 ks.

[28] See http://www.astro.isas.ac.jp/suzaku/log/hxd/.

[29] See http://suzaku.gsfc.nasa.gov/docs/suzaku/analysis/abc/; see also http://www.astro.isas.ac.jp/suzaku/analysis/.

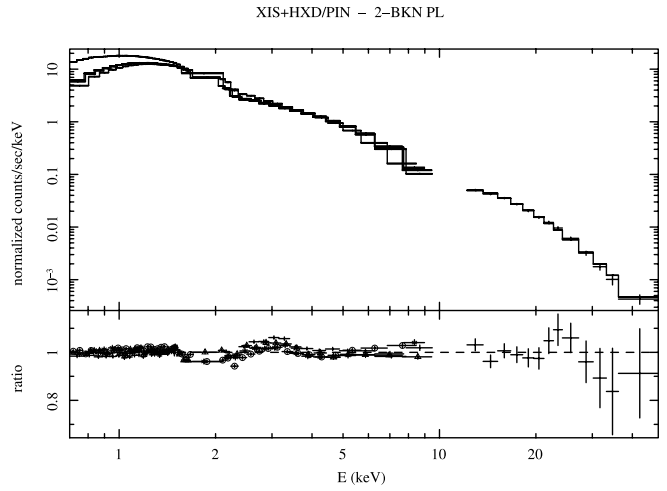

FIG. 1.—Two broken power-law model provides a good fit to the combined 4-XIS and HXD/PIN spectra. Note the good agreement between the four XIS instruments, with residuals that are of the order of only a few percent, although the high statistics of our data indicate that some systematic effects are still present in the XIS calibration. [*See the electronic edition of the Journal for a color version of this figure.*]

Response and non–X-ray background (NXB) files are directly provided by the *Suzaku* team. Note that, since the background level of HXD/PIN is extremely low, the background event files are generated with a 10 times scaled level compared to the actual background to avoid introducing a large statistical error. The EXPOSURE keyword in the background file has to be changed before the analysis. An important issue in the analysis of the HXD/PIN data concerns the estimate of the cosmic X-ray background, whose spectrum peaks in this band. We followed the procedure suggested by the *Suzaku* team (see also Kataoka et al. 2007), simulating the expected contribution of the CXB from the entire PIN field of view ($34' \times 34'$), assuming an *HEAO-1* spectrum between 3 and 60 keV (Boldt 1987; Gruber et al. 1999). At the end, the net counts represent about 10% of the total counts, with the source detected up to $\sim$50 keV. Roughly, the CXB flux account for 5% of the HXD/PIN background.

To perform a joint XIS and HXD/PIN (0.7–50 keV energy band) fit we extract XIS spectra for $t < 10^5$ s. Fitting with a broken power law as above, the PIN points lie below the model, requiring a steeper spectrum. As shown in Figure 1, a good fit is obtained using a model with three power laws (`bkn2pow` on XSPEC). This figure shows the good agreement between the four XIS instruments, with residuals that are of the order of only a few percent. Thanks to the high statistics of our data, it also indicates that some systematic effects still exist in the XIS calibration. As for the XIS-only data, to fit the continuous spectral curvature between 0.7 and 50 keV, we also used a log-parabolic law model. This provides a good fit to the joint XIS and HXD/PIN spectrum (see Table 1); however, the last few points are below the best-fitted model, indicating that above $\sim$35 keV the X-ray spectrum is decaying very rapidly, with some indication of an exponential cutoff.

2.2. *Swift*

We requested a number of observations as target of opportunity with *Swift* (Gehrels et al. 2004) around the *Suzaku* and MAGIC campaign. A total of nine short observations were carried out between 2006 May 19 and May 29. We also reanalyzed a *Swift* observation performed 1 year before, on 2005 April 19 (Tramacere et al. 2007). The source is clearly detected each time by both the X-Ray Telescope (XRT; Burrows et al. 2005) and the UltraViolet-Optical Telescope (UVOT; Roming et al. 2005), but not by the Burst Alert Telescope (BAT; Barthelmy et al. 2005); therefore, the BAT data are not included in our analysis.

2.2.1. *Swift-XRT*

The XRT data were processed using the HEASoft package. The task `xrtpipeline` was used applying the standard calibration, filtering and screening criteria, using the latest calibration files available in the *Swift* caldb distributed by HEASARC. In each observation, after a few seconds of exposure in photon counting mode, XRT automatically switched to window timing (WT) mode due to the brightness of the source. We analyzed only the WT data, selecting all the events with grades 0–2 and with energy in the range 0.3–10 keV.

Each *Swift*-XRT observation lasts for a few thousand seconds with a count rate always larger than 7 counts s^{-1}; therefore, we have good statistics for the X-ray spectrum of each observation. As in the case of the *Suzaku*-XIS spectrum, the XRT spectra are well fitted by a simple PL plus a variable interstellar absorption, with a $N_{\rm H}$ value 50% higher than the Galactic value or, if we fix the absorption to the Galactic value, by either a broken-PL model or a log-parabolic law model. In Table 2 we report the broken-PL and the log-parabolic best-fit results. Note that there is a very good match between the *Swift*-XRT and the *Suzaku*-XIS results, showing that the cross-calibration between these two instruments is quite good.

2.3. *The MAGIC Telescope*

The Major Atmospheric Gamma Imaging Cerenkov (MAGIC) telescope is an Imaging Atmospheric Cerenkov Telescope (IACT) with a 17 m diameter mirror with an energy threshold of $\sim$50 GeV. The telescope is located on the Canary Island La Palma (28.2°N, 17.8°W, 2225 m above sea level; Albert et al. 2008b).

1ES1959+650 was observed with the MAGIC telescope for 7 nights from 2006 May 21 to 27 for this campaign. The zenith angle during the observations was in the range from 36° to 43.5°. Observations were performed in wobble mode (Daum et al. 1997), where the object was observed at 0.4° offset from the camera center. After the quality selection of the data, the total effective observation time was 14.3 hr. The analysis was performed using the standard MAGIC analysis software (Albert et al. 2008b). Based on the information of shower image parameters (Hillas 1985), a multitree classification method (Random Forest) was applied for the discrimination against the dominating background of hadronic cosmic-ray events and for the energy estimation of the γ-ray events (Albert et al. 2008a). The γ-ray excess is derived from the θ^2 distribution, where the parameter θ represents the angular distance between the source position in the sky and the reconstructed arrival position of the air shower, estimated using the "DISP" method (Fomin et al. 1994).

An excess of 663 events over 5283 normalized background events yielding a significance of 7.7 σ was obtained for the spectrum calculation. Tighter cuts that only selected data with a shower image size >350 photoelectrons (corresponding to a gamma-ray energy peak of about 400 GeV) resulted in an increased 10.4 σ significance.

The measured differential energy spectrum averaged over the seven night observations by the MAGIC telescope is shown in Figure 2. It is well described by a simple power law from 150 GeV to 3 TeV, with a photon index of $\Gamma = 2.58 \pm 0.18$. The best-fit values are reported in Figure 2. Compared to the previous MAGIC measurement of 1ES1959+650 in a steady state in 2004 (Albert

TABLE 2

BEST-FIT PARAMETERS FOR THE XRT DATA OF EACH *Swift* OBSERVATION, WITH THE ABSORPTION FIXED AT THE GALACTIC VALUE, $N_{\rm H} = 10^{21}$ cm^{-2}

Date (1)	Γ_1 or a (2)	Γ_2 or b (3)	E_b (4)	χ^2_r/dof (5)	F_{2-10} (6)
Swift XRT Broken Power-Law Best Fits					
2005 Apr 19 01:05	2.00 ± 0.04	2.38 ± 0.04	$1.38^{-0.16}_{+0.13}$	0.87/369	1.2
2006 May 19 16:09	1.97 ± 0.07	2.34 ± 0.08	$1.45^{-0.30}_{+0.35}$	0.87/219	1.1
2006 May 21 03:36	1.86 ± 0.07	2.23 ± 0.05	$1.25^{-0.20}_{+0.30}$	1.09/284	1.5
2006 May 2310:09	$1.86^{-0.08}_{+0.04}$	2.14 ± 0.03	$1.15^{-0.23}_{+0.14}$	1.05/451	2.3
2006 May 24 10:33	1.86 ± 0.03	2.23 ± 0.05	$1.81^{-0.18}_{+0.18}$	0.98/374	2.4
2006 May 25 10:38	$1.86^{-0.08}_{+0.04}$	2.20 ± 0.04	$1.29^{-0.23}_{+0.15}$	1.01/439	2.0
2006 May 26 09:05	$1.68^{-0.10}_{+0.13}$	2.16 ± 0.02	$0.90^{-0.18}_{+0.04}$	1.10/439	2.0
2006 May 27 12:24	1.95 ± 0.04	2.38 ± 0.03	$1.23^{-0.11}_{+0.10}$	1.09/387	1.5
2006 May 28 01:10	1.95 ± 0.04	2.37 ± 0.03	$1.23^{-0.09}_{+0.10}$	0.99/382	1.5
2006 May 29 01:15	2.03 ± 0.04	2.42 ± 0.04	$1.23^{-0.13}_{+0.13}$	1.06/332	1.4
Swift XRT Log-parabolic Law Best Fits					
2005 Apr 19 01:05	2.09 ± 0.02	0.33 ± 0.04	...	0.88/370	1.2
2006 May 19 16:09	2.04 ± 0.03	0.34 ± 0.08	...	0.86/220	1.1
2006 May 21 03:36	1.97 ± 0.03	0.31 ± 0.06	...	1.07/285	1.5
2006 May 23 10:09	1.96 ± 0.02	0.22 ± 0.03	...	1.05/452	2.2
2006 May 24 10:33	1.89 ± 0.02	0.31 ± 0.04	...	0.95/375	2.4
2006 May 25 10:38	1.95 ± 0.02	0.29 ± 0.04	...	0.99/440	2.0
2006 May 26 09:05	2.00 ± 0.02	0.26 ± 0.04	...	1.10/440	1.9
2006 May 27 12:24	2.09 ± 0.03	0.36 ± 0.04	...	1.07/388	1.4
2006 May 28 01:10	2.08 ± 0.02	0.35 ± 0.04	...	1.03/383	1.5
2006 May 29 01:15	2.15 ± 0.02	0.33 ± 0.05	...	1.08/333	1.4

NOTE.—Col. (1): Observing date. Col. (2): Low-energy photon index for the bpl model, or log-par slope. Col. (3): High-energy photon index for the bpl model, or log-par curvature. Col. (4): Break energy (keV) for the bpl model. Col. (5): χ^2/degrees of freedom. Col. (6): Flux in the 2–10 keV band, in units of 10^{-10} erg cm^{-2} s^{-1}.

et al. 2006), the observed flux in 2006 is about 60% of the flux in 2004, while the photon indices agree within the errors.

2.4. *Swift-UVOT and Ground-based Optical Observations*

The UVOT contains three optical (UBV) and three UV (UVW1, UVM2, UVW2) lenticular filters, which cover the wavelength range between 1600 and 6000 Å. All six filters were used each time (but for the observations of 2006 May 19 and 29, when the latter UV filter was not used). The source was detected in all filters. These data were analyzed using the

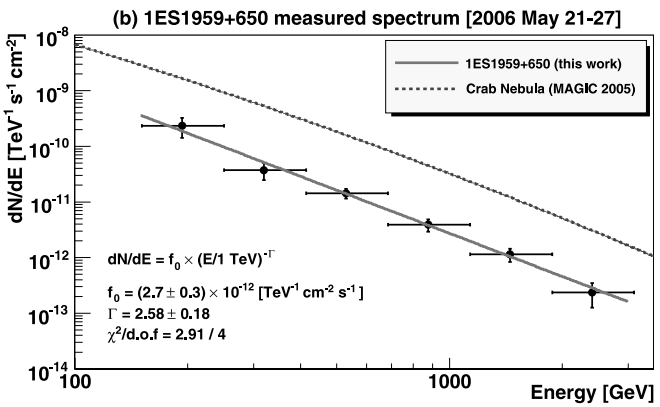

FIG. 2.—Differential energy spectrum of 1ES1959+650 as obtained by the MAGIC telescope. The spectrum is averaged over the whole data set from the 2006 campaign. The solid line represents a power-law fit to the measured spectrum. The fit parameters are listed in the figure. For comparison, the measured MAGIC Crab spectrum (Albert et al. 2008b) is shown as a dashed line. [*See the electronic edition of the Journal for a color version of this figure.*]

`uvotmaghist` task (HEASoft ver. 6.3 with calibration files updated on 2007 June 27) with a source region of 5″ for optical and 10″ for UV filters. The background was extracted from a source-free circular region with radius equal to 40″. To take into account systematic effects, we added a 10% error in flux (resulting in ~0.1 mag). In Table 3 we report the journal of the UVOT observations, the derived magnitudes, and fluxes, including the galaxy-subtracted flux values (see below).

1ES 1959+650 is one of the blazars that is regularly monitored in the Cousins *R* band with the AIT (0.40 m) of the Perugia Observatory (Tosti et al. 1996) and with both the KVA telescope on La Palma and the Tuorla 1.03 m telescope as a part of the Tuorla blazar monitoring program.[30] In Figure 3 we show the *R* light curve obtained with these telescopes during the period 2004 June to 2006 August. The observations carried out between 2006 May 5 and June 30, i.e., around our multiwavelength campaign, are reported in Table 4 and shown as an inset in Figure 3. To properly measure the optical SED of the blazar it is necessary to subtract from the observed fluxes the contribution of the underlying host galaxy, that for 1ES1959+650 is detectable even with the short focal length of our 40 cm telescope. To this end we adopted the same procedure that we applied in Tagliaferri et al. (2003) and derived the dereddened ($A_R = 0.473$, from Schlegel et al. 1998) host-galaxy subtracted fluxes of the blazar in the *R* band (we subtracted a galaxy contribution of 1.7 mJy in the *R* band; see also Nilsson et al. 2007). These values are also reported in Table 4.

We adopted the same procedure for the UVOT data, although the galaxy contribution was subtracted only for the UBV filters

[30] See http://users.utu.fi/kani/1m.

TABLE 3
Optical Properties of 1ES 1959+65 (from the UVOT Data)

Date	V (mag)	V_d (mag)	F_V (mJy)	$F_{V-\mathrm{HG}}$ (mJy)	B (mag)	B_d (mag)	F_B (mJy)	$F_{B-\mathrm{HG}}$ (mJy)
2005 Apr 19.....	14.9	14.3	5.7	4.6	15.7	14.9	4.1	3.7
2006 May 19.....	14.8	14.3	6.1	5.0	15.4	14.7	5.0	4.6
2006 May 21.....	14.8	14.2	6.3	5.2	15.4	14.7	5.2	4.8
2006 May 23.....	14.9	14.3	5.9	4.8	15.4	14.7	4.9	4.5
2006 May 24.....	14.8	14.3	6.2	5.1	15.4	14.7	5.2	4.7
2006 May 25.....	14.8	14.3	6.2	5.1	15.4	14.7	5.2	4.8
2006 May 26.....	14.8	14.2	6.6	5.5	15.4	14.6	5.3	4.8
2006 May 27.....	14.7	14.2	6.7	5.6	15.3	14.6	5.5	5.0
2006 May 28.....	14.8	14.2	6.5	5.4	15.3	14.6	5.4	5.0
2006 May 29.....	14.8	14.2	6.5	5.4	15.3	14.6	5.6	5.2
Date	U (mag)	U_d (mag)	F_U (mJy)	$F_{U-\mathrm{HG}}$ (mJy)	UVW1 (mag)	UVW1$_d$ (mag)	F_{UVW1} (mJy)	
2005 Apr 19.....	14.8	13.9	3.7	3.6	15.1	13.9	2.6	
2006 May 19.....	14.7	13.8	4.0	3.9	15.0	13.8	2.9	
2006 May 21.....	14.6	13.7	4.3	4.2	14.9	13.7	3.1	
2006 May 23.....	14.7	13.8	4.1	4.0	15.0	13.8	2.9	
2006 May 24.....	14.6	13.7	4.3	4.2	14.9	13.7	3.1	
2006 May 25.....	14.6	13.7	4.3	4.2	14.9	13.7	3.1	
2006 May 26.....	14.6	13.7	4.4	4.3	14.9	13.7	3.1	
2006 May 27.....	14.6	13.6	4.6	4.5	14.8	13.6	3.3	
2006 May 28.....	14.6	13.7	4.5	4.4	14.8	13.6	3.3	
2006 May 29.....	14.5	13.6	4.7	4.6	14.8	13.6	3.3	
Date	$UVM2$ (mag)	$UVM2_d$ (mag)	F_{UVM2} (mJy)	UVW2 (mag)	UVW2$_d$ (mag)	F_{UVW2} (mJy)		
2005 Apr 19.....	15.0	13.6	2.8	15.0	13.3	3.5		
2006 May 19.....	15.0	13.5	3.0					
2006 May 21.....	14.9	13.5	3.1	14.9	13.2	3.9		
2006 May 23.....	14.9	13.5	3.1	14.9	13.2	3.9		
2006 May 24.....	14.9	13.4	3.2	14.8	13.1	4.2		
2006 May 25.....	14.9	13.4	3.3	14.8	13.1	4.2		
2006 May 26.....	14.8	13.4	3.3	14.8	13.1	4.2		
2006 May 27.....	14.9	13.4	3.2	14.8	13.0	4.5		
2006 May 28.....	14.8	13.4	3.4	14.8	13.1	4.3		
2006 May 29.....	14.8	13.3	3.6					

Notes.—The data are averaged over the pointings of each day. The 1 σ uncertainties in the parameter estimates, including systematics, are of 10% in flux (corresponding to about 0.1 mag). Shown for each filter are the observed magnitude, dereddened magnitude, and monochromatic flux. The monochromatic flux subtracted from the contribution of the host galaxy is calculated only for the optical filters, since this is negligible at the UV frequencies.

(for the galaxy contribution in these filters we used the "standard" colors for an elliptical galaxy following Fukugita et al. 1995), given that it is negligible in the UV filters.

3. RESULTS

The good agreement between the *Suzaku* and *Swift* XRT results is shown in Figure 4, where we report the highest and the lowest X-ray status as recorded by XRT, together with the X-ray spectrum observed by *Suzaku*, which is near to the higher status. Note that we do not have strictly simultaneous spectra; therefore, we did not attempt to simultaneously fit the *Suzaku* and *Swift*-XRT data. The wide-energy range of *Suzaku* simultaneously includes the broad peak and the following rapid decay of the synchrotron component. This together with the optical/UV data of *Swift* and on-ground observations allow us to properly monitor the synchrotron component of the SED. In Figure 5 we plot all nine X-ray spectra observed by XRT from 2006 May 19 to May 29. Besides the variability of a factor of 2 in flux, this figure clearly shows that the peak of the synchrotron component, which is well within the XRT band (0.3–10 keV), moves to higher energies with the increasing flux. Moreover, it is also evident that the flux at higher energies, i.e., above the synchrotron peak, increases and decreases more rapidly than the fluxes at lower energies, a behavior that has already been noted in other HBLs (e.g., Ravasio et al. 2004; Brinkmann et al. 2005; Zhang et al. 2005). This is also confirmed by the *Suzaku* observation. In fact, during this long monitoring of more than 2 days, the source also showed some rapid variability. Figure 6 reports the soft (0.2–2 keV) and hard (2–10) X-ray light curves of 1ES 1959+650 as recorded with the XIS1. The data track a flare of small amplitude ($\sim$10%) with a rising time of $t_r \simeq 20$–30 ks. The variability is faster in the 2–10 keV band than in the 0.2–2 keV band, as also shown by the hardness ratio (*bottom panel*); note in particular the sudden drop visible at $t \simeq 1.5 \times 10^5$ s. Again, this is in agreement with the behavior shown by the XRT data (i.e., higher variability at energies above the synchrotron peak).

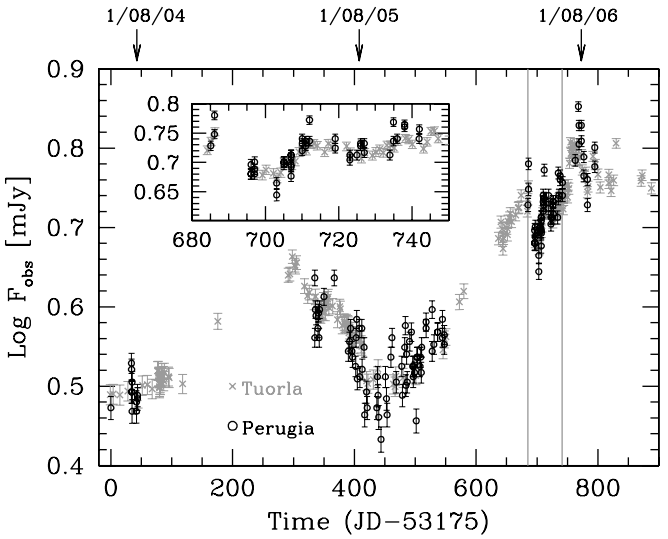

FIG. 3.—*R* optical light curve recorded with the AIT-Perugia telescope and with both the KVA telescope on La Palma and the Tuorla 1.03 m telescope as a part of the Tuorla blazar monitorin program during the period 2004 June to 2006 August. The data reported in the figure are just the observed values and are not corrected for either the galactic absorption or the host galaxy contribution (in order to have a better match, for plotting reasons, we subtracted a value of 0.05 from the Tuorla and KVA values in this plot). The inset shows the light curve between the two vertical lines, whose values are also reported in Table 4 (note that in this table we did not subtract the constant value as in the figure) and that are centered around the X-ray and VHE observations. [*See the electronic edition of the Journal for a color version of this figure.*]

Our optical (*R*-band) monitoring from 2004 June to 2006 August shows that the source was in a relatively active state (see Fig. 3). During the more intense monitoring of 2006 May–June, centered around our multiwavelength campaign, the source showed a variability of 0.1–0.2 mag around a mean value of 14.4 (including the galaxy). In particular, in the period May 25–June 1, the *R*-flux increased by ∼40% (see Table 4 and inset of Fig. 3), at odds with the 2–10 keV X-ray flux that instead shows a decrease in the period May 25–29. This can again be explained by the synchrotron peak moving at lower energies (i.e., to the left side): the X-ray flux after the peak decreases, while the optical flux, which is before the peak, increases. During the *Swift* 10 day monitoring, the source remained constant in the UVOT filters at values that are the same as the one recorded 1 year before (see Table 3) and that are fully consistent with the fluxes observed in the *R* band (see Figs. 4 and 8). Given the uncertainties of the UVOT measurements, with these data we can say that the source did not vary by more than 50% in the UVOT filters during this period. Clearly, the source is more variable in the soft X-ray band, about a factor of 2 on a timescale of days (see Table 2 and Fig. 4). This is not surprising for HBLs, which are known to be highly variable in this band. In fact, if we look at the SED reported in Figure 4, we can see that the synchrotron component peaks between 1 and 2 keV; therefore, it is natural that we should see more variability in the X-ray than in the optical-UV band (of course if variability is caused by a spectral change above the peak).

In the VHE band the average integrated flux above 300 GeV is $(1.27 \pm 0.16) \times 10^{-11}$ cm^{-2} s^{-1}, which corresponds to about 10% of the Crab Nebula flux. This corresponds to one of the lowest levels so far observed in the VHE band, about a factor of 2 lower than the lowest flux detected previously both with HEGRA in the years 2000–2001 and MAGIC in 2004 and well below the highest level detected in 2002 May (Aharonian et al. 2003; Albert et al. 2006). The diurnal light curves of VHE γ-rays

TABLE 4

OPTICAL PROPERTIES OF 1ES 1959+65

Date	R (mag)	R_d (mag)	F_R (mJy)	$F_{R\text{–HG}}$ (mJy)
	Perugia Observations			
2006 May 5.....	14.40 ± 0.03	13.93	8.3	6.6 ± 0.2
2006 May 6.....	14.31 ± 0.04	13.84	9.0	7.3 ± 0.3
2006 May 16.....	14.51 ± 0.04	14.03	7.5	5.8 ± 0.3
2006 May 17.....	14.50 ± 0.04	14.02	7.6	5.9 ± 0.3
2006 May 23.....	14.59 ± 0.06	14.11	7.0	5.3 ± 0.4
2006 May 25.....	14.47 ± 0.04	14.00	7.7	6.1 ± 0.3
2006 May 27.....	14.47 ± 0.04	14.00	7.7	6.1 ± 0.3
2006 May 30.....	14.39 ± 0.04	13.92	8.3	6.6 ± 0.3
2006 May 31.....	14.39 ± 0.03	13.92	8.3	6.7 ± 0.2
2006 Jun 1	14.33 ± 0.03	13.86	8.8	7.1 ± 0.2
2006 Jun 8	14.39 ± 0.03	13.92	8.3	6.7 ± 0.2
2006 Jun 12	14.45 ± 0.03	13.98	7.9	6.2 ± 0.2
2006 Jun 13	14.44 ± 0.04	13.98	8.0	6.3 ± 0.3
2006 Jun 14	14.39 ± 0.04	13.92	8.3	6.6 ± 0.3
2006 Jun 15	14.41 ± 0.03	13.94	8.2	6.5 ± 0.2
2006 Jun 22	14.44 ± 0.07	13.98	8.0	6.3 ± 0.5
2006 Jun 23	14.34 ± 0.06	13.87	8.7	7.1 ± 0.4
2006 Jun 24	14.37 ± 0.04	13.90	8.5	6.8 ± 0.3
2006 Jun 26	14.31 ± 0.04	13.84	8.9	7.3 ± 0.3
2006 Jun 30	14.37 ± 0.03	13.90	8.5	6.8 ± 0.2
	Tuorla Observations			
2006 May 05.....	14.26 ± 0.02	13.78	9.4	7.7 ± 0.1
2006 May 06.....	14.22 ± 0.02	13.74	9.8	8.1 ± 0.1
2006 May 17.....	14.39 ± 0.02	13.92	8.4	6.7 ± 0.1
2006 May 19.....	14.40 ± 0.02	13.93	8.3	6.6 ± 0.1
2006 May 20.....	14.38 ± 0.02	13.90	8.4	6.7 ± 0.1
2006 May 22.....	14.39 ± 0.02	13.92	8.3	6.6 ± 0.1
2006 May 23.....	14.41 ± 0.02	13.94	8.2	6.5 ± 0.1
2006 May 24.....	14.39 ± 0.02	13.92	8.4	6.7 ± 0.1
2006 May 25.....	14.35 ± 0.02	13.88	8.7	7.0 ± 0.1
2006 May 25.....	14.34 ± 0.02	13.87	8.7	7.0 ± 0.1
2006 May 27.....	14.36 ± 0.02	13.88	8.6	6.9 ± 0.1
2006 May 28.....	14.34 ± 0.02	13.87	8.7	7.0 ± 0.1
2006 May 29.....	14.30 ± 0.02	13.83	9.1	7.4 ± 0.1
2006 May 30.....	14.30 ± 0.02	13.82	9.1	7.4 ± 0.1
2006 May 31.....	14.30 ± 0.02	13.82	9.1	7.4 ± 0.1
2006 Jun 01	14.27 ± 0.02	13.80	9.3	7.6 ± 0.1
2006 Jun 02	14.27 ± 0.02	13.79	9.4	7.7 ± 0.1
2006 Jun 03	14.28 ± 0.02	13.80	9.3	7.6 ± 0.1
2006 Jun 05	14.30 ± 0.02	13.83	9.1	7.6 ± 0.1
2006 Jun 06	14.27 ± 0.02	13.79	9.4	7.7 ± 0.1
2006 Jun 07	14.28 ± 0.02	13.80	9.3	7.6 ± 0.1
2006 Jun 11	14.28 ± 0.02	13.80	9.3	7.6 ± 0.1
2006 Jun 12	14.30 ± 0.02	13.83	9.1	7.6 ± 0.1
2006 Jun 15	14.33 ± 0.02	13.86	8.8	7.1 ± 0.1
2006 Jun 16	14.31 ± 0.02	13.83	9.0	7.3 ± 0.1
2006 Jun 18	14.32 ± 0.02	13.84	8.9	7.2 ± 0.1
2006 Jun 19	14.30 ± 0.02	13.83	9.1	7.6 ± 0.1
2006 Jun 20	14.29 ± 0.02	13.82	9.2	7.5 ± 0.1
2006 Jun 21	14.31 ± 0.02	13.83	9.0	7.3 ± 0.1
2006 Jun 22	14.27 ± 0.02	13.80	9.3	7.6 ± 0.1
2006 Jun 23	14.27 ± 0.02	13.80	9.3	7.6 ± 0.1
2006 Jun 24	14.28 ± 0.02	13.81	9.2	7.5 ± 0.1
2006 Jun 25	14.26 ± 0.02	13.78	9.4	7.7 ± 0.1
2006 Jun 27	14.24 ± 0.02	13.77	9.6	7.9 ± 0.1
2006 Jun 28	14.25 ± 0.02	13.78	9.5	7.8 ± 0.1

NOTES.—The data are averaged over the pointings of each day. The 1 σ uncertainties in the parameter estimates. The columns indicate the date, observed magnitude, dereddened magnitude, monochromatic flux, and monochromatic flux minus the contribution of the host galaxy.

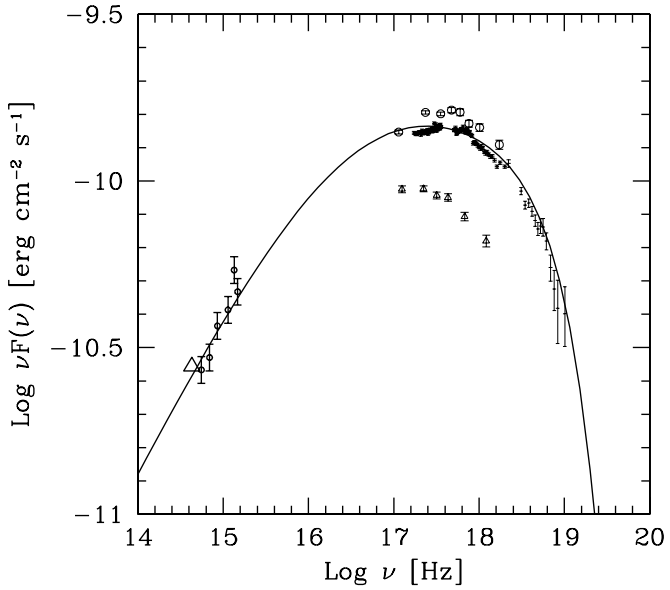

FIG. 4.—Highest and lowest optical-UV-X-ray status of 1ES 1959+650 as observed by *Swift* during the period 2006 May 19–29. Note that, while in the X-ray band there is a variability of a factor of 2, in the optical the source does not vary significantly. For comparison, we also report the averaged X-ray spectrum as observed by *Suzaku* on 2006 May 23–25, which is consistent with the higher XRT spectrum observed on May 24. The wider energy range of *Suzaku* constrains very well the synchrotron component of the SED, around and after the synchrotron peak. [*See the electronic edition of the Journal for a color version of this figure.*]

above 300 GeV are shown in Figure 7; no significant strong variability can be seen. However, due to the low source flux level, we could only have seen variability of a factor of 2–3.

4. DISCUSSION AND CONCLUSIONS

The full SED of 1ES 1959+650 as measured at the end of 2006 May is reported in Figure 8, together with other historical data. During our multiwavelength campaign, we simultaneously observed the SED from the optical, to the UV, soft and hard X-rays, and VHE bands, monitoring both the synchrotron and Compton components. The historical data in this figure show very strong changes in the X-ray band, while in the optical this is much more attenuated, a behavior that is also found in the results obtained from our observing campaign.

During our multiwavelegth campaign the source is found to be in a high state with respect to the historical behavior in both X-ray and optical (e.g., Tagliaferri et al. 2003; see Fig. 3), although not at the highest state as observed in the X-ray (e.g., Holder et al. 2003b; see Fig. 8). In the VHE band, instead, the source is at one of the lowest states so far recorded. We also found that the X-ray fluxes at energies above the synchrotron peak vary more rapidly than the X-ray fluxes below the peak. Also, the VHE band shows historical strong variability, particularly if we consider that in this band there are fewer observations than in the optical or X-ray ones. However, from our data we do not see strong (i.e., a factor of 2–3) variability in the VHE band. Our MAGIC data are probably monitoring the part of the SED slightly above the peak of the Compton component. Therefore, one would expect to see a high level of variability. The lack of variability in the MAGIC data and the low flux level recorded both indicate that the source was not very active in this band. Overall we can say that during our campaign the source was quite stable (i.e., did not vary by more than a factor of 2) from the optical to the VHE band.

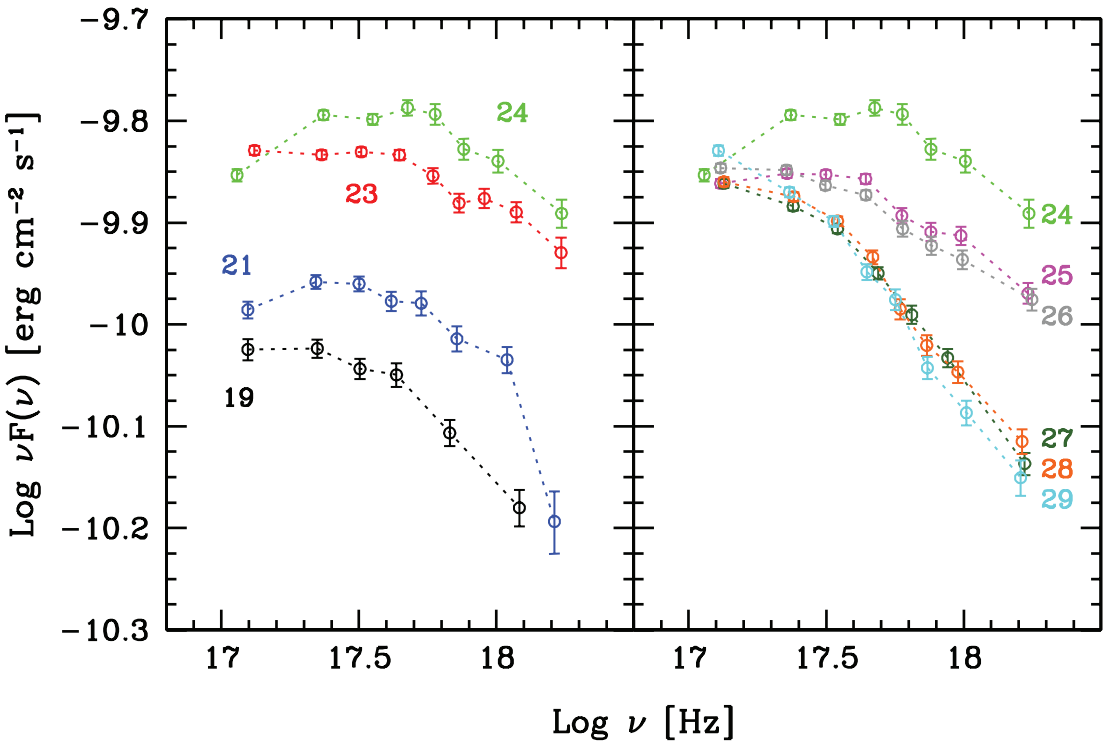

FIG. 5.—The 0.3–7 keV X-ray spectrum as derived from the *Swift* XRT observations of 2006 May 19–29. In the left panel the flux increases from one spectrum to the next one (observations of May 19, 21, 23, and 24). On the contrary, in the right panel the flux decreases from one spectrum to the next one (observations of May 24, 25, 26, 27, and 28). Note how the synchrotron peak moves to higher energies with the flux increase (*left panel*) and that the flux at higher energies varies more rapidly than the fluxes at lower energies, in particular in the right panel.

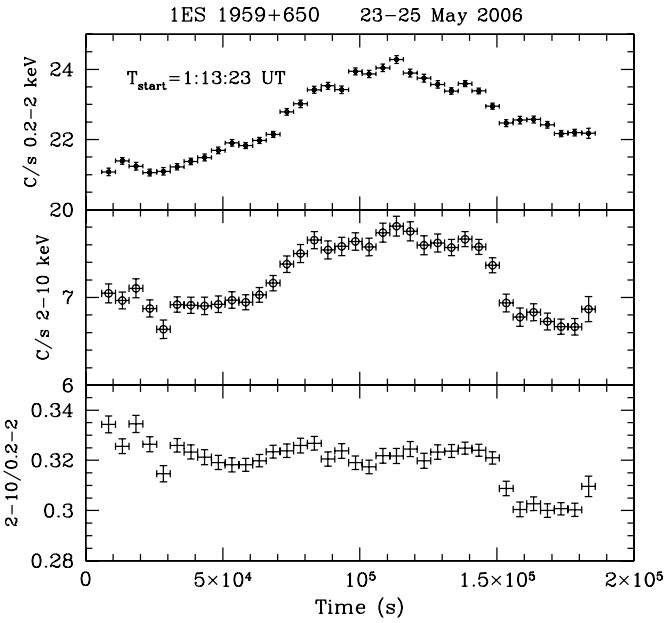

FIG. 6.—*Suzaku*-XIS1 soft (0.2–2 keV) and hard (2–10) X-ray light curves. The small amount of variability detected (∼10%) is faster at the higher energies, as also shown by the hardness ratio (*bottom panel*).

The observed X-ray variability behavior allows a few interesting considerations about the properties of the emitting regions. First, note that the variability is not random but follows a rising/decay trend on a timescale of ∼10 days (see the *Swift* XRT results). In this observed time Δt, a single blob moving with a bulk Lorentz factor $\Gamma \sim 18$ (see below) moves by a distance $\Delta z \sim c\Delta t\Gamma^2 \sim 2.7$ pc. Therefore, we cannot assume that we are observing a single moving blob traveling that far, since the blob would expand, lose energy by adiabatic losses, and change (decrease) its magnetic field. This in turn would decrease the produced flux and would lengthen the variability timescale. Also, the internal shock model (Spada et al. 2001; Guetta et al. 2004) cannot explain the variability we are observing. In fact, in this model the radiation is produced in a shock resulting from the collision of two shells moving at slightly different velocities. In this case the variability is predicted to be erratic; therefore, to explain the variability we have seen we have to finely tune the different Γ of the shells. We are thus led to consider the possibility that the observed radiation originates in the same region of the jet, through some kind of "standing shock." For instance, we might think of the interaction of a fast spine and a shear layer occurring at about the same distance from the central powerhouse (see Ghisellini et al. [2005] for mode details, including the possibility of radiative deceleration of the spine through the "Compton rocket" effect in TeV blazars). A "standing shock" scenario has already been proposed by Krawczynski et al. (2002) in order to explain the tight correlation between X-ray and TeV flares observed in Mrk 501, and it is also discussed in some detail by Sokolov et al. (2004).

As we did with the previous multiwavelength observing campaigns on 1ES 1959+650 that we organized based on the *BeppoSAX* observations (Tagliaferri et al. 2003), we can try to fit our SED with a homogeneous, one-zone synchrotron inverse Compton model. During the *BeppoSAX* campaigns, in order to derive the SSC physical parameters, we had to assume a value for the Compton component, which we derived by rescaling a non-simultaneous VHE spectrum based on the X-ray flux. This time we also have the VHE observations; therefore, both SSC components are constrained by real data. As shown in Figure 8, the X-ray spectrum as observed by *Suzaku* and *Swift* is about a factor of 2 higher than the one measured with *BeppoSAX*, and also the synchrotron peak has moved to somewhat higher energy, confirming the previous results of a higher energy peak with higher fluxes (e.g., Tagliaferri et al. 2003), which is typical for HBLs (see the dramatic case of Mrk 501; Pian et al. 1998). The optical fluxes are similar to the one reported for the 2002 SED. The observed VHE spectrum is similar to, but lower than, that of the 2002 SED. In summary, the 2006 SED has optical fluxes that are similar to those of 2002; the X-ray fluxes are a factor of 2 higher and the VHE fluxes are a factor of ∼2 lower. In the assumed one-zone SSC model, the source is a sphere with radius R moving with bulk Lorentz factor Γ and seen at an angle θ by the observer, resulting in a Doppler factor δ. The magnetic field is tangled and uniform, while the injected relativistic particles are assumed to have a (smooth) broken power-law spectrum with normalization K, extending from $\gamma_{\rm min}$ to $\gamma_{\rm max}$ and with indexes n_1 and n_2 below and above the break at γ_b. Assuming this model, the SED of 2006 May can be well represented using the following parameters: $\delta = 18$, $R = 7.3 \times 10^{15}$ cm, $B = 0.25$ G, $K = 2.2 \times 10^3$ cm^{-3}, and an electron distribution extending from $\gamma_{\rm min} = 1$ to $\gamma_{\rm max} = 6.0 \times 10^5$, with a break at $\gamma_b = 5.7 \times 10^4$ and slopes $n_1 = 2$ and $n_2 = 3.4$. The intrinsic luminosity is $L' = 5.5 \times 10^{40}$ erg s^{-1}. If we compare these values with the one we derived for the 2002 SED (although in that case we use a slightly different emission model), we see that the parameters are very similar, with a source that is slightly more compact, a lower magnetic field, and an almost identical Doppler factor. Similar values are also found to

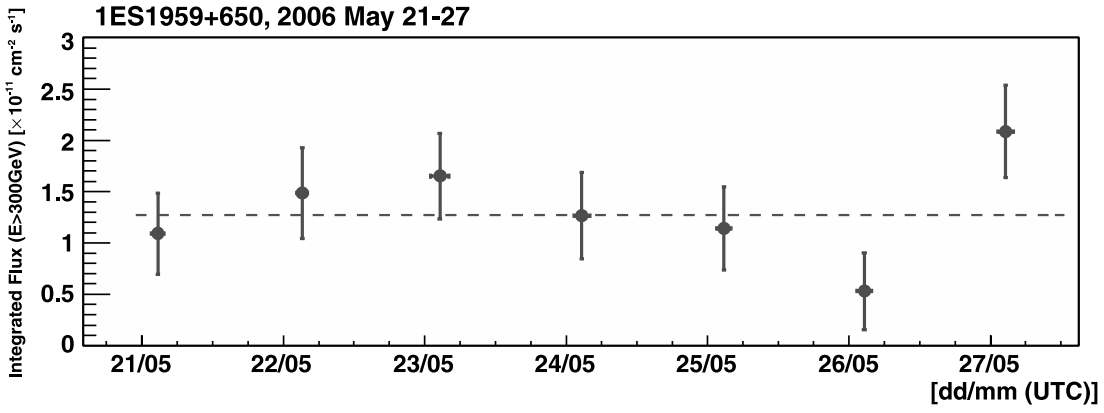

FIG. 7.—Diurnal VHE ($E > 300$ GeV) light curve of 1ES1959+650 from the MAGIC observations. A horizontal dashed line indicates the average flux level during the campaign. [*See the electronic edition of the Journal for a color version of this figure.*]

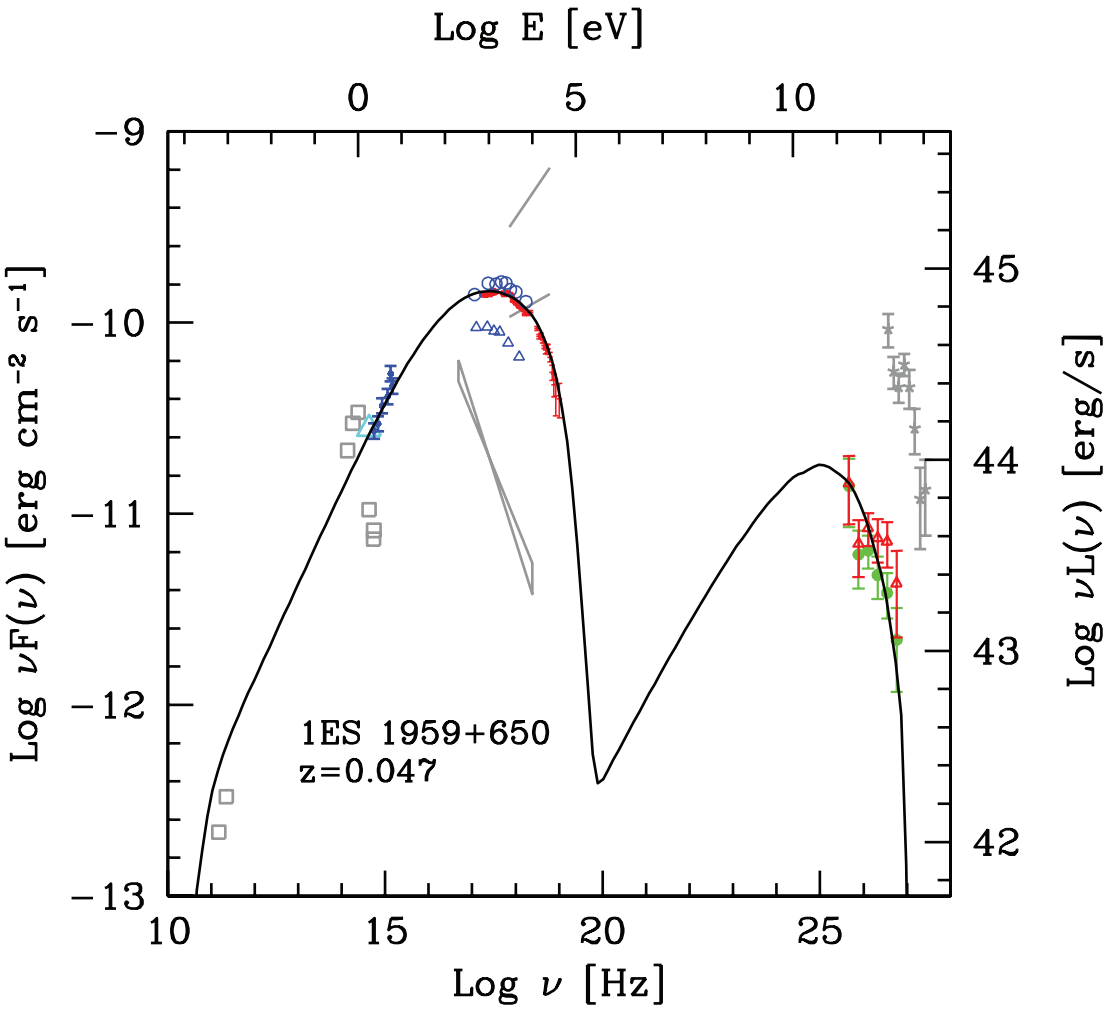

FIG. 8.—SED of 1ES 1959+650 as measured at the end of 2006 May, together with other historical data. Optical-UV data are from on-ground (*cyan triangle*) and UVOT/*Swift* (*blue triangles*). The average *Suzaku* spectrum (*red*) and the *Swift* spectra taken on May 24 and May 29 are reported. Green points (*filled circles*) report the observed MAGIC spectrum, while the red points (*open triangles*) have been corrected for the absorption by the IR background using the "low model" of Kneiske et al. (2004). Historical data are taken from Tagliaferri et al. (2003, radio-optical), Krawczynski et al. (2002, X-rays), Beckmann et al. (2002, X-rays), and Aharonian et al. (2003, TeV, highest level). The line reports the synchrotron+SSC model (see text). The spectra reported for the X-ray and TeV bands correspond to the highest and lowest flux so far recorded for this source in these bands.

explain the SED of PKS 2155−304 during and after the strong TeV flare observed in 2006 July; however, in that case we found less steep slopes for the electrons and a higher value of δ (see Foschini et al. 2007). Once again, the physical parameters that we derived assuming a one-zone SSC model are typical of HBL objects. Finally, the historical SEDs of 1ES1959+650 show that in this source the synchrotron emission is dominating above the Compton one.

We thank Neil Gehrels and the whole *Swift* team for the ToO observations and the *Suzaku* team for their assistance in the analysis of our *Suzaku* data. We thank the IAC for the excellent working conditions at the ORM. We acknowledge financial support from the ASI-INAF contract I/088/06/0. The MAGIC project is supported by the German BMBF and MPG, the Italian INFN, the Spanish CICYT, the Swiss ETH Research Grant TH34/04, and the Polish MNiI Grant 1P03D01028.

REFERENCES

Aharonian, F., et al. 2003, A&A, 406, L9
———. 2007, ApJ, 664, L71
Albert, J., et al. 2006, ApJ, 639, 761
———. 2008a, Nucl. Instrum. Methods Phys, Res. A, 588, 424
———. 2008b, ApJ, 674, 1046
Barthelmy, S., et al. 2005a, Space Sci. Rev., 120, 143
Becker, R. H., White, R. L., & Edwards, A. L. 1991, ApJS, 75, 1
Boldt, E. 1987, in IAU Symp. 124, Observational Cosmology, ed. A. Hewitt, G. Burbidge, & L. Z. Fang (Dordrecht: Reidel), 611
Böttcher, M. 2007, Ap&SS, 309, 95
Brinkmann, W., Papadakis, I. E., Raeth, C., Mimica, P., & Haberl, F. 2005, A&A, 443, 397
Buckley, J. H., et al. 1996, ApJ, 472, L9
Burrows, D. N., et al. 2005, Space Sci. Rev., 120, 165
Catanese, M., et al. 1997, ApJ, 487, L143
Daum, A., et al. 1997, Astropart. Phys., 8, 1
Donato, D., Sambruna, R. M., & Gilozzi, M. 2005, A&A, 433, 1163
Elvis, M., Plummer, D., Schachter, J., & Fabbiano, G. 1992, ApJS, 80, 257
Falomo, R., Kotilainen, J. K., & Treves, A. 2002, ApJ, 569, L35
Fomin, V. P., et al. 1994, Astropart. Phys., 2, 137
Foschini, L., et al. 2007, ApJ, 657, L81
Fossati, G., Maraschi, L., Celotti, A., Comastri, A., & Ghisellini, G. 1998, MNRAS, 299, 433
Fukugita, M., Shimasaku, K., & Ichikawa, T. 1995, PASP, 107, 945
Gehrels, N., et al. 2004, ApJ, 611, 1005
Ghisellini, G., Celotti, A., Fossati, G., Maraschi, L., & Comastri, A. 1998, MNRAS, 301, 451
Ghisellini, G., Tavecchio, F., & Chiaberge, M. 2005, A&A, 432, 401

Giebels, B., et al. 2002, ApJ, 571, 763
Gregory, P. C., & Condon, J. J. 1991, ApJS, 75, 1011
Gruber, D. E., Matteson, J. L., Peterson, L. E., & Jung, G. V. 1999, ApJ, 520, 124
Guetta, D., Ghisellini, G., Lazzati, D., & Celotti, A. 2004, A&A, 421, 877
Gutierrez, K. J., et al. 2006, ApJ, 644, 742
Hayashida, M., et al. 2008, in Proc. 30th Int. Cosmic Ray Conf. (Merida), in press (arXiv:0709.2349)
Heidt, J., Nilsson, K., Sillanpää A., Takalo, L. O., & Pursimo, T. 1999, A&A, 341, 683
Hillas, A. M. 1985, in Proc. 29th Int. Cosmic Ray Conf. (La Jolla), 445
Holder, J., Bond, I. H., Boyleet, P. J., et al. 2003a, ApJ, 583, L9
Holder, J., et al. 2003b, in Proc. 28th Int. Cosmic Ray Conf. (Tsukuba), 2619
Kataoka, J., et al. 2007, PASJ, 59, 279
Kneiske, T. M., Bretz, T., Mannheim, K., & Hartmann, D. H. 2004, A&A, 413, 807
Koyama, K., et al. 2007, PASJ, 59, S23
Krawczynski, H., Coppi, P. S., & Aharonian, F. 2002, MNRAS, 336, 721
Krawczynski, H., et al. 2004, ApJ, 601, 151
Maraschi, L., et al. 1999, ApJ, 526, L81
Massaro, E., Perri, M., Giommi, P., & Nesci, R. 2004, A&A, 413, 489
Mitsuda, K., et al. 2007, PASJ, 59, S1
Nilsson, K., et al. 2007, A&A, 475, 199
Padovani, P., & Giommi, P. 1995, ApJ, 444, 567
Pian, E., Vacanti, G., Tagliaferri, G., et al. 1998, ApJ, 492, L17
Punch, M., et al. 1992, Nature, 358, 477
Ravasio, M., Tagliaferri, G., Ghisellini, G., & Tavecchio, F. 2004, A&A, 424, 841
Roming, P. N., et al. 2005, Space Sci. Rev., 120, 95
Schlegel, D. J., Finkbeiner, D. P., & Davis, M. 1998, ApJ, 500, 525
Sokolov, A., Marscher, A., P., & McHardy, I. M. 2004, ApJ, 613, 725
Spada, M., Ghisellini, G., Lazzati, D., & Celotti, A. 2001, MNRAS, 325, 1559
Takahashi, T., et al. 2007, PASJ, 59, S35
Tagliaferri, G., Ravasio, M., Ghisellini, G., Tavecchio, F., Giommi, P., Massaro, E., Nesci, R., & Tosti, G. 2003, A&A, 412, 711
Tavecchio, F., Maraschi, L., & Ghisellini, G. 1998, ApJ, 509, 608
Tavecchio, F., Maraschi, L., Ghisellini, G., Kataoka, J., Foschini, L., Sambruna, R. M., & Tagliaferri, G. 2007, ApJ, 665, 980
Tosti, G., Pascolini, S., & Fiorucci, M. 1996, PASP, 108, 706
Tramacere, A., et al. 2007, A&A, 467, 501
von Montigny, C., et al. 1995, ApJ, 440, 525
Zhang, Y. H., Treves, A., Celotti, A., Qin, Y. P., & Bai, J. M. 2005, ApJ, 629, 686